ADVANCED FUNCTIONAL MATERIALS

www.afm-journal.de

Photo-and Electroluminescence from Nitrogen-Doped and Nitrogen–Sulfur Codoped Graphene Quantum Dots

*Md Tanvir Hasan, Roberto Gonzalez-Rodriguez, Conor Ryan, Nicolas Faerber, Jeffery L. Coffer, and Anton V. Naumov**

As opposed to inorganic counterparts, organic quantum dots often exhibit lower fluorescence efficiencies and are complex to synthesize. Here we develop nitrogen-doped (N-GQDs) and nitrogen–sulfur codoped (NS-GQDs) graphene quantum dots exhibiting high-yield visible and near-IR emission that are synthesized via a single-step microwave-assisted hydrothermal technique with a single glucosamine-HCl starting material (thiourea precursor used for NS-GQDs). As-synthesized N-GQDs and NS-GQDs are well-dispersed (average sizes of 5.50 and 3.90 nm) with high crystallinity and pronounced G-band. Formed by the bottom-up assembly of glucosamine, they contain amine linkage and a variety of oxygen-containing functional groups assessed by Fourier-transform infrared spectroscopy with ≈2% sulfur for NS-GQDs. The synthetic procedure allows varying their size and the bandgap. Unlike other graphene-based quantum dots, these GQDs exhibit bright, stable fluorescence both in the visible and near-IR with high quantum yields of up to 60%. Excitation-dependent visible fluorescence is attributed to size-dependent bandgaps, with near-IR emission potentially arising from the emissive defect states/their arrangements. Advantageous properties of these GQDs are utilized to develop exciton recombination layer for organic light-emitting devices exhibiting both photoluminescence and electroluminescence in the visible. Produced by ecofriendly one-step scalable synthesis brightly-emissive N-GQDs and NS-GQDs become a promising material for novel organic optoelectronics.

1. Introduction

Graphene is a 2D material that offers a wide variety of electronic applications as it possesses remarkable electrical/thermal conductivity, high transparency, superior tensile strength, and high thermal/chemical stability.[1–5] However, it cannot be used as an emissive material for optoelectronics or bioimaging applications due to its band structure of a zero-gap semiconductor. Graphene-derived functionalized and confined materials such as graphene oxide (GO), graphene quantum dots (GQDs), and graphene nanoribbons emit fluorescence (FL),[6–11] which makes them suitable for a wider range of optical applications. GO has the advantages of a large heavily functionalized platform for further modification, however, it exhibits a broad emission with a lower quantum yield on the order of 1%.[12,13] GQDs are known to have a more ordered uniform structure with size-confined bandgaps[14–17] and generally exhibit higher quantum yields[18,19] required for optical emissive devices and biological fluorescence probes. These 0D carbon-based species are known to have stable FL,[20] not prone to photobleaching, low cytotoxicity,[21,22] good biocompatibility,[21,23] high water solubility,[22] some pH sensitivity,[24] and low aggregation affinity. Possessing all these advantageous properties, GQDs have significant potential to advance critical areas of modern technology including light-emitting devices (LEDs),[25–27] photovoltaics,[28–30] fluorescent bioimaging,[31,32] biosensing,[33,34] pH sensing,[35,36] photoelectrocatalysis,[37,38] etc. As of now, several synthesis methods have been established to produce GQDs including hydrothermal cutting method from graphene oxide,[39] electrochemical exfoliation suitable for large-scale production,[40,41] pulsed-laser-induced photochemical stitching,[42] multistep organic synthesis yield well-defined structures and various sizes of GQDs,[43] solvothermal method involving single-step synthesis procedure,[32] nanolithography approach to form a designed pattern,[44] amidative cutting of tattered graphite to control the size of GQDs by varying amine concentration,[45] etc.

Depending on the method of synthesis and size-tuning of GQDs, the fluorescence can be either strongly

Md T. Hasan, Dr. R. Gonzalez-Rodriguez, C. Ryan, Prof. A. V. Naumov
Department of Physics and Astronomy
Texas Christian University
TCU Box 298840, Fort Worth, TX 76129, USA
E-mail: a.naumov@tcu.edu
N. Faerber
Institute of Physics
The University of Augsburg
86135 Augsburg, Germany
Prof. J. L. Coffer
Department of Chemistry and Biochemistry
Texas Christian University
TCU Box 298860, Fort Worth, TX 76129, USA
The ORCID identification number(s) for the author(s) of this article can be found under https://doi.org/10.1002/adfm.201804337.

DOI: 10.1002/adfm.201804337

excitation-wavelength-dependent over a broad range (350–800 nm),[46–48] or exhibit only a slight to negligible dependence for a shorter wavelength (300–470 nm) range.[49,50] This is supported by Yeh et al.[51] and Kwon et al.[45] reporting that fine-tuning of GQDs' size can lead to excitation wavelength-independent emission. Most of those materials exhibit only a single transition and moderate quantum yields.[51–53]

Recently, carbon-based quantum dots were synthesized from graphene oxide via a top-down approach showing a high quantum yield of 74%.[18] These provide an advantageous alternative to inorganic quantum dots,[54,55] however, may still have rather complex and costly preparation for device mass fabrication. Additionally, only a single transition in the visible is observed with this material. More simplistic bottom-up synthetic approaches with a few starting materials also provide similarly structured carbon quantum dots however with a lower quantum yield of only 6.42%.[56] More complex routes not optimized for device fabrication produce higher yield QDs,[57,58] however, those result only in a single emission feature in the visible. For optoelectronics and bioimaging applications we seek a new method to enhance the quantum yields of such QDs, and at the same time simplify the synthetic procedure to make it scalable and allow for emission at multiple wavelengths: in the visible and near-infrared (NIR).

In this work, we for the first time use a bottom-up approach with single glucosamine hydrochloride (glucosamine-HCl) starting material to produce nitrogen-doped graphene quantum dots (N-GQDs), via a microwave-assisted single-step hydrothermal method. Similar but thiourea-driven synthesis is used to produce nitrogen–sulfur codoped graphene quantum dots (NS-GQDs). This procedure provides ≈5.5 and ≈3.9 nm average sized N-GQDs and NS-GQDs with the high quantum yields of 22–60% and two optical transitions: in the visible and near-infrared. The synthesis procedure of N-GQDs/NS-GQDs is straightforward, less time consuming and requires fewer resources than for their top-down synthesized counterparts allowing for mass production for device applications. The source of precursor material is widely available and inexpensive.

In addition to cost efficiency and simplicity in fabrication, as opposed to existing counterparts,[59–61] these novel quantum dots exhibit emission in both visible and near-infrared. PL mechanism of such GQDs remains controversial even after a number of scientific reports in this field: it is attributed to such routes as recombination of electron–hole pair originated from localized sp^2 graphitic carbon platform surrounded by functionalized sp^3 carbon,[62] size-dependent quantum confinement effects,[63,64] emissive defect states,[49,63,65] or surface passivation.[47,49] In this study, we propose that N-GQDs/NS-GQDs emission originates from the combination of quantum confined states (size distribution of GQDs) and potentially, the distribution of emissive trap states associated with functional groups or surface passivation by amino/thiol groups originated in the hydrothermal synthesis. Different dopant structures are used in this work to explore the influence of the dopant type on the optical and electronic properties of quantum dots. As a result, N-GQDs and NS-GQDs synthesis resulted in the materials emissive both in the visible and NIR and suitable for optoelectronic applications. We fabricate LED devices considering N-GQDs and NS-GQDs as active layers to explore the potential optoelectronic device applications of GQDs. N-GQDs and NS-GQDs have excellent aqueous solution stability as well as tunable electronic structure, which allows for inexpensive fast-produced LEDs providing potential advantage over inorganic GaN-devices.[66] Additionally, the use of highly fluorescent nitrogen and sulfur-doped GQDs in organic electroluminescence (EL) devices may avoid the use of rare earth element-based Iridium complex as a dopant material.[67]

2. Results and Discussion

N-GQDs/NS-GQDs are synthesized by microwave treatment (at 450W) of aqueous glucosamine-HCl or glucosamine-HCl with thiourea. These precursor materials undergo a hydrothermal process in the presence of continuous uniform microwave treatment for 40 min yielding well-distributed GQDs in a stable aqueous suspension. The simplicity and low cost of the synthetic procedure with just a single-step single-compound reaction for N-GQDs suggests a possibility of efficient mass production of these quantum dots for commercial applications. For this study, glucosamine-HCl is used as the source of carbon and nitrogen dopants to produce N-GQDs. Alternatively, in the synthesis of NS-GQDs, both the glucosamine and thiourea act as a source of carbon. In addition to that, thiourea works as a catalyst for the dehydration process and provides nitrogen and sulfur for doping. With microwave treatment, the dehydration takes place due to the reaction among monomeric glucosamine molecules forming a polymeric chain to produce N-GQDs. Thiourea further introduces nitrogen/sulfur dopants to the glucosamine polymeric chain yielding NS-GQDs. After the polymerization, nucleation takes place followed by doping of nitrogen/nitrogen–sulfur to form N-GQDs/NS-GQDs. Formation/growth of carbon nuclei is verified by the crystalline structure images of GQDs captured by high-resolution transmission electron microscope (HRTEM). This growth mechanism of GQDs is illustrated in **Figure 1** via a schematic diagram. The reaction rate to produce GQDs is predicted to be power-dependent and may be significantly increased with higher powers of microwave radiation (>450 W). However, to avoid the possibility of rapid water evaporation and spill/overflow of a solution containing precursor materials, a power over 450 W is not considered.

After the 40 min microwave treatment, both N-GQDs/NS-GQDs exhibit a dramatic color change from the starting colorless solution to yellow and pink/orange respectively (Inset of **Figure 2**c,f), suggesting the formation of new materials including a change in the structural/optical properties compared to the starting ones. In order to eliminate the excess of unreacted precursor materials, GQDs are dialyzed in a 0.5–1 kDa molecular-weight-cutoff dialysis bag for a week prior to further characterization.

HRTEM is used to characterize the morphology, distribution, and crystallinity of the newly synthesized GQDs. The TEM study indicates that the GQDs are not only individualized and well-dispersed (Figure 2a,d) but also well-distributed as shown by the size distribution analysis in the histogram plot (Figure 2c,f). We consider ≈100 of GQDs to calculate the

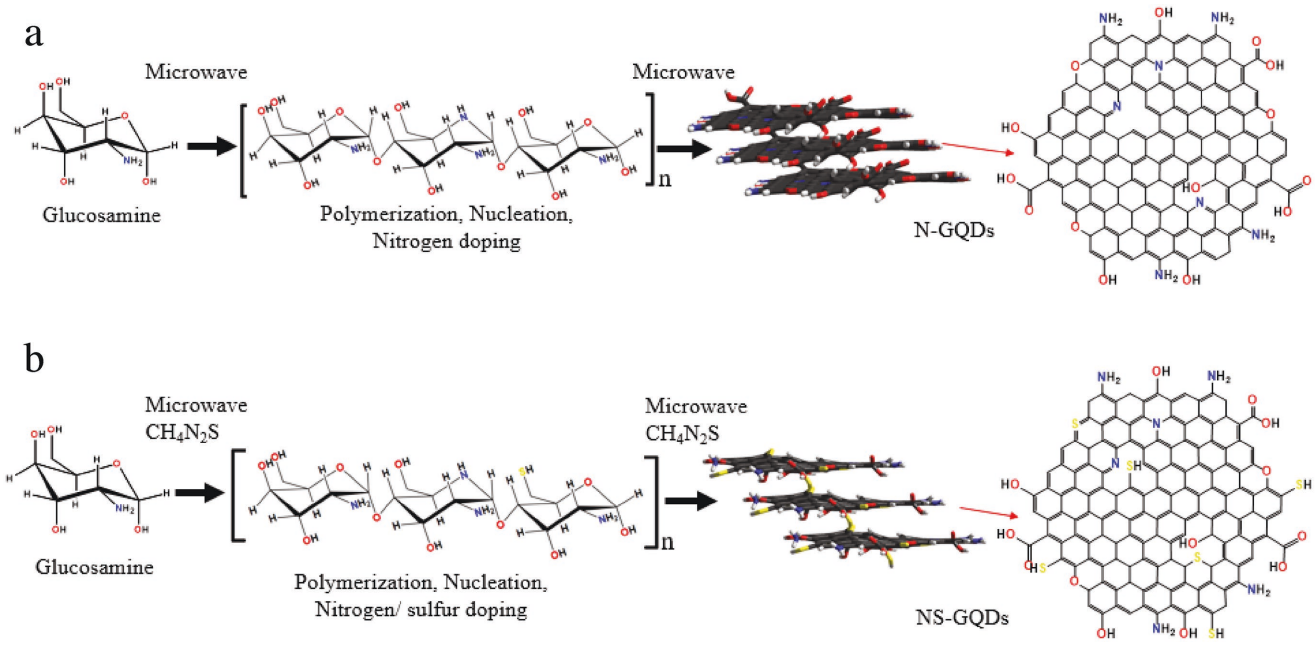

Figure 1. Schematic of the growth mechanism of a) N-GQDS and b) NS-GQDs.

average size (diameter) of each type. The calculated average size is 5.5 nm with a range of 1.61 nm to 9 nm for N-GQDs and a 3.9 nm average size within a range of 1.91–6.22 nm for NS-GQDs. The HRTEM images of N-GQDs (Figure 2b) and NS-GQDs (Figure 2e) reveal discernible lattice fringes with a spacing of 0.21 nm between them (Inset of Figure 2b,e) corresponding to (100) plane of graphene.[15]

It also shows high crystalline lattice structure apparent in the fast-Fourier-transform (FFT) images of the chosen area (Inset of Figure 2b,e). The presence of nitrogen in N-GQDs and NS-GQDs and sulfur in NS-GQDs is assessed qualitatively via energy-dispersive X-ray spectroscopy (EDX) analysis showing approximate percent fractions of 11 and 8% for nitrogen and 2% for sulfur (Figure S1, Supporting Information). The thickness of GQDs was measured with atomic force microscope (AFM) showing up to ≈2.5 nm for N-GQDs (Figure 2g) and ≈1.75 nm for NS-GQDs (Figure 2h) on average which suggests the multilayered and potentially spherical structure of GQDs.

Fourier-transform infrared spectroscopy (FTIR) of N-GQDs/NS-GQDs performed in attenuated total reflectance (ATR) mode with freeze-dried, dehydrated material shows the bands at 3275, 3090 cm^{-1} (**Figure 3**a,b) that can be attributed to the stretching vibrations of O—H and N—H groups, respectively, with a well-pronounced presence of the O—H.[68] The peaks centered at 2935, 1602, 1530, and 1412 cm^{-1} correspond to the vibrational transitions of C—H, C=O of COOH, C=C, C—O—C. Additionally, stretching vibrations of C—OH, C—N/N—H/C—H, and C—O are detected at 1330, 1240, and 1021 cm^{-1}, respectively.[49,68] All these peaks are common for both types of GQDs except C—S, S—H stretching peaks/shoulders at 1159, 2557 cm^{-1}[69–71] for NS-GQDs. However, the intensity of these peaks/shoulders is very low because of the low sulfur content detected qualitatively by EDX. The presence of these transitions confirms the functional groups assumed in the proposed structures (Figure 1). Addition of more functionalities via reaction with thiourea could contribute to more intense transitions for NS-GQDs. Raman spectroscopy is used to characterize the graphitic structure within the GQDs showing a sharp G-band at ≈1537 cm^{-1} corresponding to the sp2-hybridized carbons and a weak shoulder at ≈1330 cm^{-1} (D band) indicating a presence of some disordered structure (Figure S2a,b, Supporting Information).

The morphology of synthesized N-GQDs/NS-GQDs and their functional group content determine their optical properties that are assessed in this work by UV–vis and fluorescence spectroscopy. The UV–vis spectra (**Figure 4**e) of N-GQDs show absorption peak centered at 275 nm that can be attributed to a red-shifted π–π^* transition of C=C bond with two weak shoulders at 306, 366 nm representing two n–π^* transitions at C=O and C=N.[8,72] On the other hand, NS-GQDs show stronger absorption band (Figure 4e) at 236 nm consistent with π–π^* transition of C=C bond[71] and weak shoulders at 276, 300, and 370 nm as the potential signature of n–π^* transitions in C=O and C=N bonds. The shifts in absorption spectra between two types of quantum dots are likely related to the presence of sulfur dopants in NS-GQDs reflecting the interaction of the major absorbing species on the sp^2 platform with the dopants. Such interaction mechanisms govern the fluorescence emission in these QDs as the fluorescing species appear not to be the major absorbers: fluorescence is excited in the visible far from major absorption transitions.

Fluorescence spectroscopy shows substantial emission features in two spectral regions: visible and NIR for both the N-GQDs and NS-GQDs. In order to account for the emission induced by π–π^* and n–π^* absorption transitions,[48] the excitation wavelength is varied from 280 to 340 nm showing multiple emission peaks (Figure S4, Supporting Information). As the excitation wavelength increases, these additional peaks get weaker/disappear suggesting lower fluorescence contribution from π–π^* and n–π^* transitions finally (at 330/340 nm

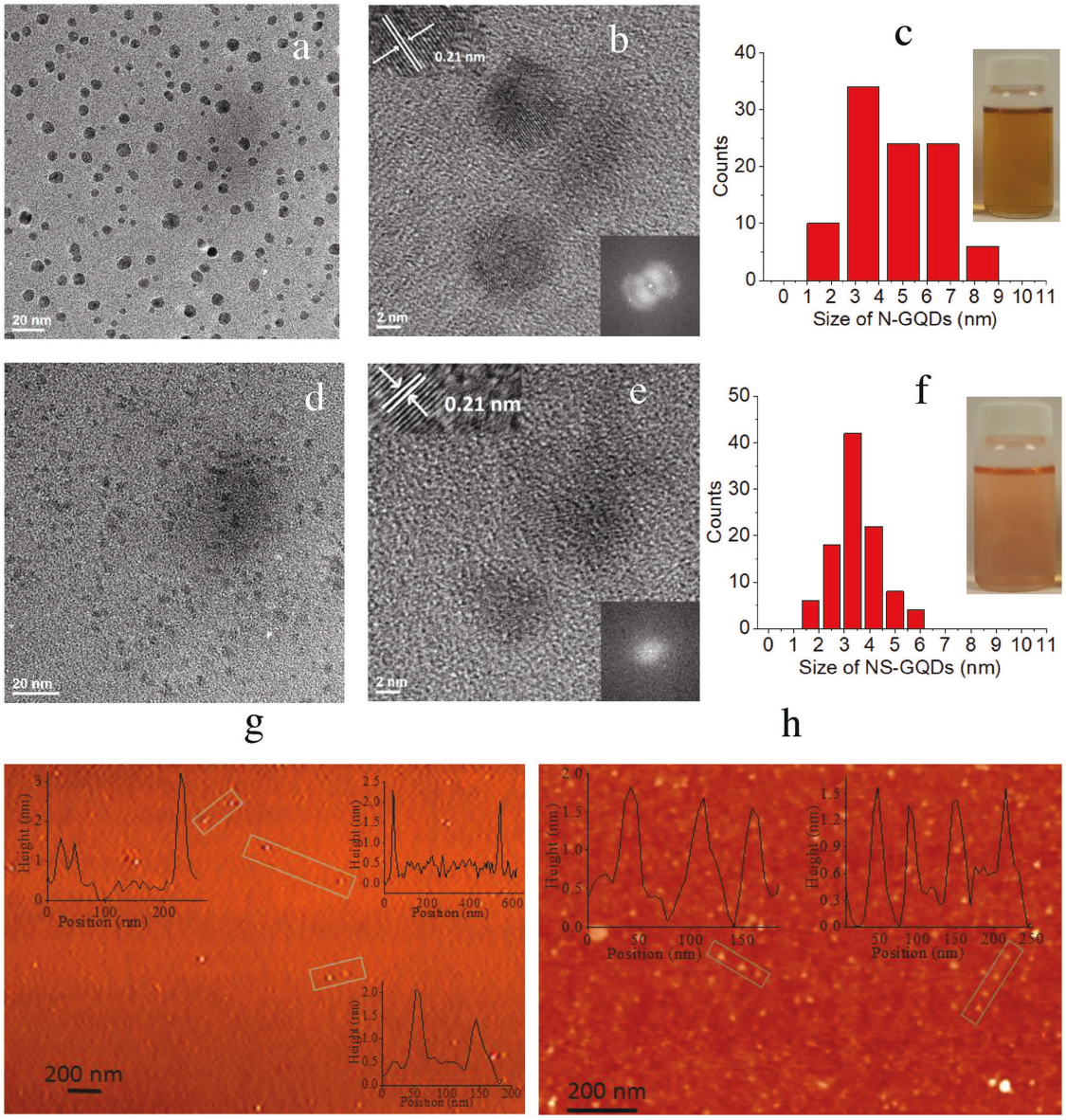

Figure 2. TEM images showing the distribution of a) N-GQDS, d) NS-GQDs. HRTEM images of b) N-GQDs, e) NS-GQDs. Inset: separation between lattice fringes and FFT images of selected area. Size distribution of c) N-GQDs, f) NS-GQDs. Inset: As prepared respective GQD samples. AFM height profile for g) N-GQDs and h) NS-GQDs.

excitation) resulting into one broad fluorescence feature further explored in this work. For NS-GQDs this transition occurs at longer excitation wavelengths as consistent with more redshifted absorption spectral features. This broader feature shows direct excitation dependence: scanning excitation from 350 to 475 nm allows to tune the emission in the visible from 425 to 531 nm for N-GQDs (Figure 4a) and 448 to 539 nm for NS-GQDs (Figure 4c) with similar behavior observed in NIR emission (Figure 4b,d). We also measure the photoluminescence with a variation in excitation wavelength from 500 to 675 nm (Figure S3, Supporting Information) showing redshifted fluorescence peak maxima with the increase of excitation wavelength. At the NIR excitation of 700 to 800 nm, we observe emission ranging from ≈800 to 890 nm (Figure 4b,d). The emission intensity for both visible and NIR decreases with excitation wavelength. This indicates the presence of multiple sizes/types of emissive features. Blue/green emission occurring with over 340 nm excitation is usually attributed to the confinement-induced bandgap dictated by the size of the quantum dots[73] and is thus expected to vary with QDs size. As excitation is shifted, different sizes are excited in resonance, therefore providing shifted emission with the probability of exciting more species at higher excitation energies. Since only limited size-distributions of both QDs are observed, the excitation-dependent NIR emission could potentially arise from different distribution/arrangements of emissive trap states.[74,75] Such defect trap states can be associated with functional groups present in both N-GQDs/NS-GQDs.[74,75] In thiourea-driven

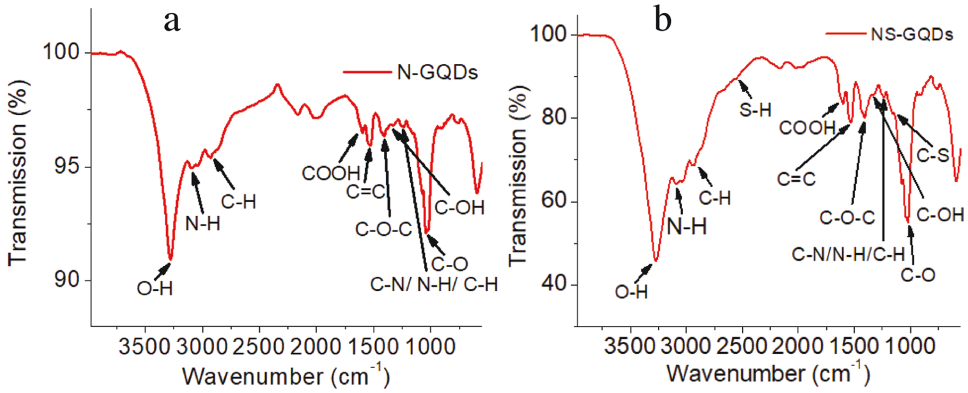

Figure 3. FTIR spectrum of a) N-GQDs and b) NS-GQDs.

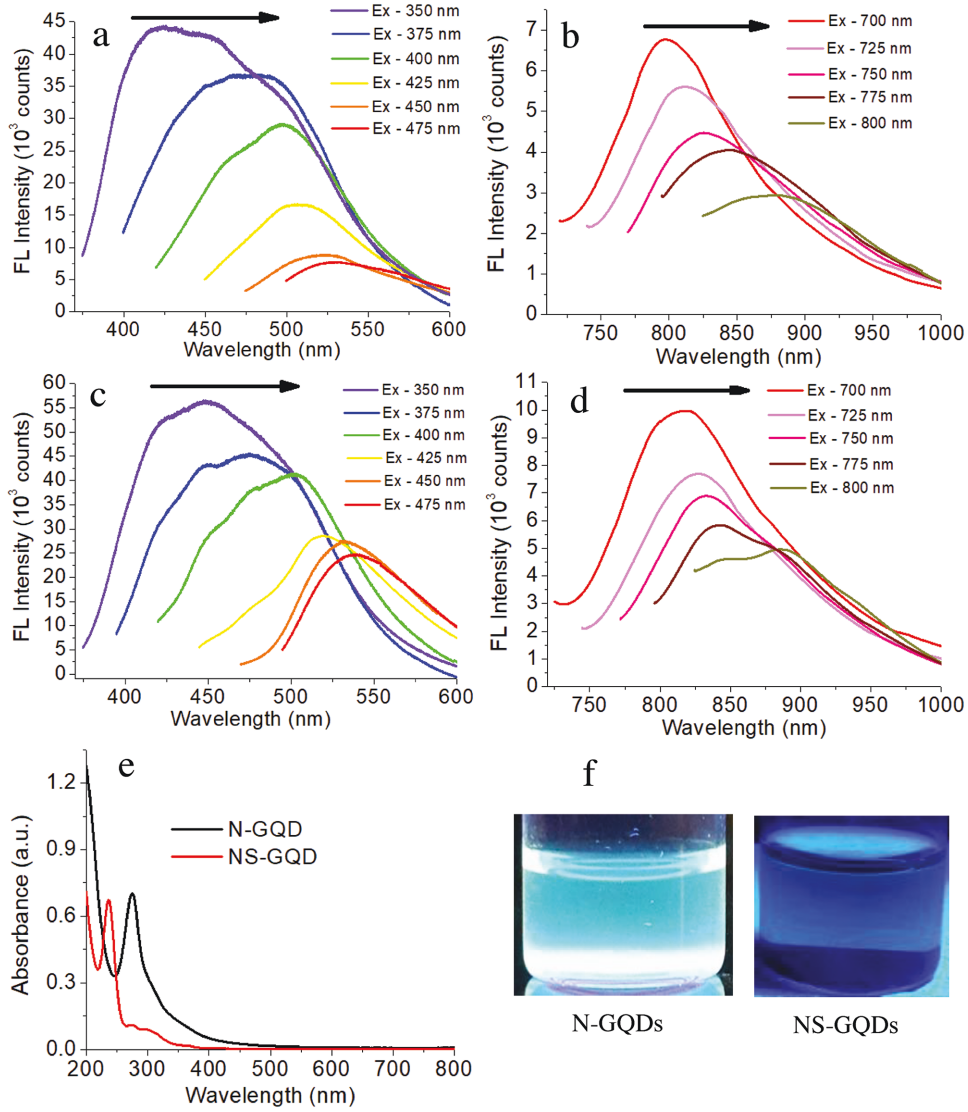

Figure 4. Excitation-dependent emission in a) visible, b) NIR from N-GQDs, c) visible, and d) NIR from NS-GQDs. e) Absorbance spectra of N-GQDs and NS-GQDs. f) Cyan and blue emission from the respective as prepared N-GQDs and NS-GQDs under the illumination of a 365 nm UV lamp.

NS-GQDs synthesis amino/thiol groups are expected to passivate the trap states[76] on the surface to reduce/diminish the excitation dependence. However, a high-power microwave treatment at 450 W may result in high local temperatures preventing surface passivation with amino/thiol groups that are unstable at higher temperatures leaving the surface of GQDs.[76] This may allow both N-GQDs/NS-GQDs exhibit excitation-dependent emission in NIR. The fluorescence is stable over the period of several hours with no signs of photobleaching. A cyan-like and blue fluorescence are also observed visually (Figure 4f) when N-GQDs and NS-GQDs are irradiated by a 365 nm 100W UV lamp suggesting a high fluorescence efficiency.

We assess the fluorescence quantum yield (QY) of N-GQDs/NS-GQDs by using a comparative method[77] choosing Coumarin-153 and Fluorescein as two standard materials with excitation and emission wavelengths similar to those of QDs. Both standards show similar results with estimated QY ranging from 50 to 60% for N-GQDs and from 10 to 22% for NS-GQDs (Figure S5, Supporting Information). The lower quantum yield of NS-GQDs, as opposed to N-GQDs, could be the consequence of the additional nonradiative pathways introduced by sulfur dopants. Therefore, considering the same concentration of both types of GQDs, NS-GQDs show less intense fluorescence along with no significant change in absorbance compared to N-GQDs resulting in lower quantum yield. Multicolor emission and, nevertheless, substantial quantum yield suggest quantum dots prepared in this work as promising materials for applications in optoelectronics and biomedicine.

The effect of the microwave treatment time on the emission and size of GQDs is explored via TEM and fluorescence study: GQDs prepared with 20, 40, and 80 min of microwave treatment show increase in average GQDs size (Figures S6 and S7, Supporting Information) and visible fluorescence shifts with longer microwave treatment. The fluorescence intensity also increases with treatment time suggesting an increase in the concentration of GQDs confirmed qualitatively with TEM. The fluorescence peak maxima show observable redshift ≈30 nm for N-GQDs (Figure S8a, Supporting Information) and ≈24 nm for NS-GQDs (Figure S8c, Supporting Information) in the visible, whereas no significant shift is detected in the NIR region (Figure S8b,d, Supporting Information) for both GQDs. Redshift in the visible fluorescence points to QD size-derived band structure, whereas the lack of change in the NIR response with treatment affecting GQD size suggests that NIR emission does not originate from GQD size confinement effects rather arising from the localized electronic environments induced by the defect states at the functional groups.

The potential effect of dopant concentration on the optical properties of GQDs was assessed via varying the amount of initial dopant-containing precursor. Nitrogen content is not expected to be altered in the present synthesis, thus, with the increase of precursor amount, the concentration of N-GQDs increases leading to a higher emission intensity without any significant shift in fluorescence maxima (Figure S9a,b, Supporting Information). With the increase of sulfur dopants in the synthesis of NS-GQDs through varying thiourea concentration, the emission intensity in the visible decreases (Figure S9c, Supporting Information), whereas NIR emission gets enhanced up to glucosamine/thiourea molar ratio of 1:1 (Figure S9d, Supporting Information) and further diminishes. However, no significant shifts in the emission maxima (visible and NIR) are observed for any variation of the precursor/dopant concentration. We expect that the increase of sulfur dopant concentration creates more defect sites which introduce additional nonradiative pathways leading to a decrease in emission intensity in the visible (Figure S9c, Supporting Information). This is likely a reason for having lower quantum yield from NS-GQDs as compared to N-GQDs. However, a higher number of defect states could lead to an increase in NIR emission potentially arising from those states (Figure S9d, Supporting Information) competing with nonradiative quenching.

Although variation in sulfur precursor concentration only affects the emission intensity, we anticipate that varying dopant concentration together with dopant type (e.g., phosphorus, boron, etc.) or codoping may allow tuning the NIR emission features in both intensity and spectral position. Also, surface passivation with additional functional groups (e.g., amino, thiol, etc.)[47,76] may adjust the electronic environment of the aforementioned defects further affecting the position/intensity of NIR feature.

In order to explore the optoelectronic device applications of these GQDs we fabricate LED devices consisting of 150 nm Indium tin oxide (ITO)-coated glass as anode coated by a hole injection layer of poly(3,4-ethylene dioxythiophene):poly(styrene sulfonate) (abbreviated as PEDOT:PSS) with a thickness of 200 nm, and then by the emissive dopant layer of N-GQDs or NS-GQDs, topped by the silver-based cathode (**Figure 5**a, and Figure S10a, Supporting Information). A cross-section of the device verifying the layered structure is observed with the scanning electron microscope (Figure S11, Supporting Information). The corresponding energy diagram (Figure 5b, and Figure S10b, Supporting Information) shows the feasibility of separate electron and hole transport from one electrode to the other through the emissive quantum dot layers. For a given potential, holes are injected from the PEDOT: PSS and electrons from the silver into the recombination layer consisting in N-GQDs or NS-GQDs.

Bright electroluminescence emission is detected from both types of devices placed inside the chamber of Horiba Nanolog Spectrofluorometer through the transparent ITO electrodes. In this system (Figure 5c, and Figure S10c, Supporting Information), we show a representative EL spectrum of ITO/PEDOT:PSS/N-GQDs and ITO/PEDOT:PSS/NS-GQDs at a fixed bias of 12 V at room temperature. EL spectra from these devices exhibit same peak positions under liquid nitrogen (LN) at a fixed bias of 12 V (Figure 5d, and Figure S10d, Supporting Information) as emission was collected from LN-cooled devices inside the spectrometer. This confirms the electronic nature of the observed transitions. Additionally to that, a number of peak maxima in EL spectra resemble those in fluorescence spectra acquired from the devices (Figure 5f, and Figure S10f, Supporting Information) with minor to no spectral shifts between the two. With different types of dopants, the device shows variation in the optoelectronic properties which can be potentially attributed to the dopants yielding defect states with different electronic environments acting as potential electron traps with distinct energy level structure.

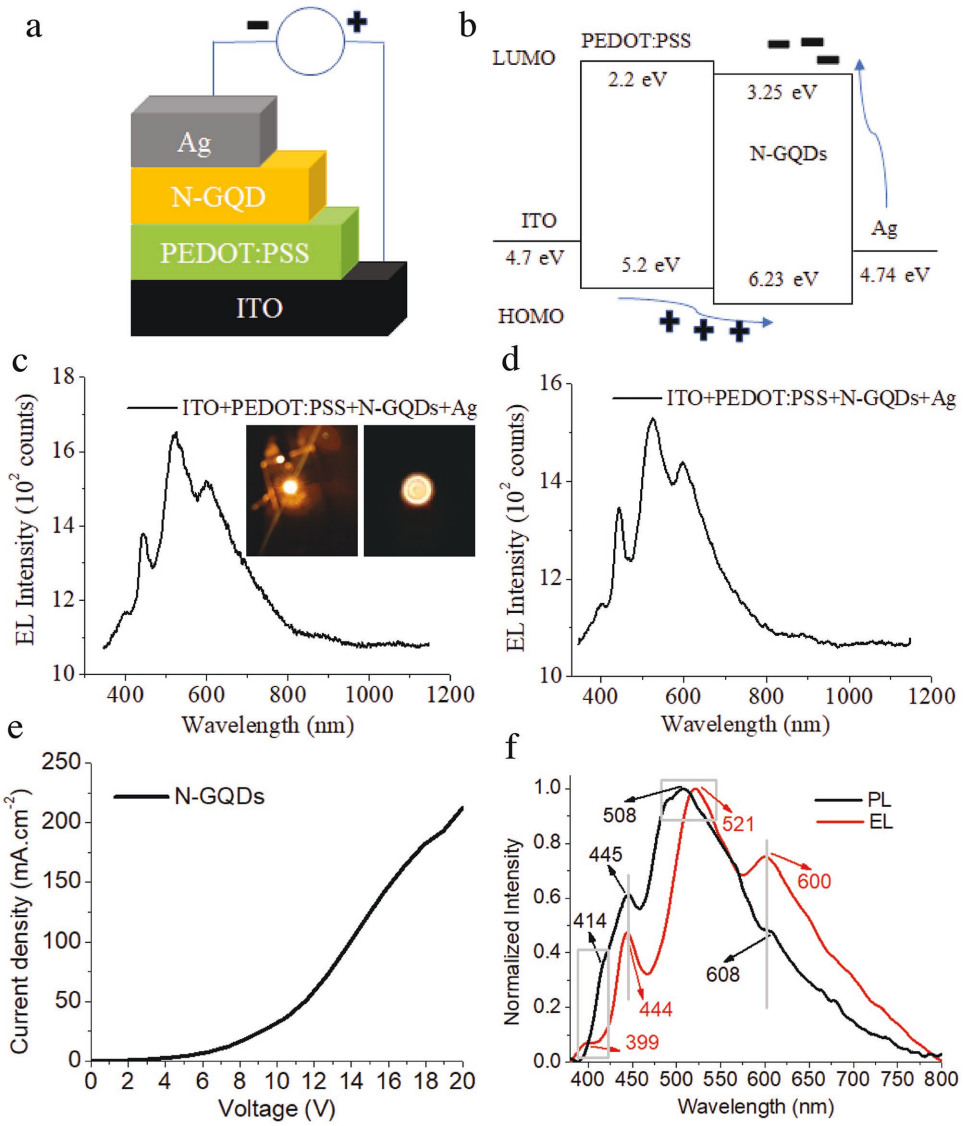

Figure 5. a) Schematic and b) illustrative energy band diagram for N-GQDs based LED device. Electroluminescence response from N-GQDs based device under c) room temperature and d) cryogenic temperature. e) Current density–voltage (*J–V*) characteristics for the device fabricated with N-GQDs. f) Comparison of photoluminescence (PL) and electroluminescence (EL) measurement spectra of LEDs fabricated with N-GQDs.

In this EL process, the holes in the HOMO of the quantum dots are recombined with electrons in the LUMO. There are O, N, and S states in the LUMO that are related to π^* orbitals of C=O, C=N, and C=S (for NS-GQDs), while the holes in HOMO are localized in the n orbitals of C=O, C=N and C=S (for NS-GQDs) and π orbitals in C=C.[70] Electronic transitions between these states result in electroluminescence. Consistent with this mechanism EL spectra of ITO/PEDOT: PSS/N-GQDs show four main peaks (Figure 5c) at 400 nm (3.09 eV), 441 nm (2.81 eV), 524 nm (2.37 eV), and 600 nm (2.07 eV) and EL spectra of ITO/PEDOT:PSS/NS-GQDs exhibit three notable peaks (Figure S10c, Supporting Information) at 406 nm (3.05 eV), 445 nm (2.79 eV), and 583 nm (2.13 eV). The peaks around 3 eV for ITO/PEDOT: PSS/N-GQDs and ITO/PEDOT: PSS/NS-GQDs are likely due to the bandgap of PEDOT: PSS, while the other three main peaks of ITO/PEDOT: PSS/N-GQDs at 2.8, 2.37, and 2.07 eV may correspond to the O and N states.[70] In the case of ITO/PEDOT: PSS/NS-GQDs, we observe the peaks at 2.79 eV, and 2.13 eV that correspond to O and S states, as expected from sulfur doping and in addition a small broad peak between 2.79 and 2.13 eV potentially due to the N state in the NS-GQDs. The strongest peaks at 3.0 and 2.79 eV are consistent with the violet-blue (inset of Figure S10c, Supporting Information) emission of ITO/PEDOT: PSS/NS-GQDs observed by the naked-eye. A schematic of the corresponding energy band diagram of O, N, and S states has shown in Figure S12 (Supporting Information). We consider the Fermi level of the GQDs as 4.74 eV based on the Kelvin Probe data by Kwon et al.[45] shown to be independent of QDs size for similarly structured graphene quantum dots. Values of HOMO and LUMO are assessed with respect to midgap Fermi energy and the bandgap size calculated directly from fluorescence peak

maxima of GQDs produced in this work. The devices are tested at different voltages with the moderate turn-on voltage of ≈7 V (Figure 5e, and Figure S10e, Supporting Information) for both devices, and only the intensity changes in the EL spectra are observed with no apparent spectral shifts. It also provides evidence that these GQD-based EL devices can be fabricated with other luminosity related parameters to be analyzed in future studies. This work provides a new one-step synthesis of GQDs with high quantum yields for applications in nanoscale imaging and also presents a versatile, low-cost alternative for the fabrication of effective EL devices.

3. Conclusion

In summary, we utilize a simple single-step microwave-facilitated hydrothermal method to synthesize N-GQDs (average size ≈5.5 nm) and nitrogen–sulfur codoped graphene quantum dots (NS-GQDs: average size ≈3.9 nm) from glucose-based inexpensive precursor materials. These novel quantum dots form stable water suspensions and exhibit bright and stable fluorescence in the visible and near-infrared with up to 60% high quantum yields. We suggest that the excitation-dependent visible emission is dictated by the QDs size-dependent bandgaps, whereas the emission in the NIR can be attributed to the trap states and their arrangements created by multiple surface functionalities that can also be related to the QDs size. We utilize these quantum dots to successfully fabricate light-emitting devices showing bright electroluminescence in the visible. GQDs, energy level structures, make them suitable as an effective electron–hole recombination medium. Considering their high quantum yield, ability to emit electroluminescence and low-cost one-step preparation, N-GQDs and NS-GQDs can be potentially used for biological imaging and, as shown in this work, as a basis for novel optoelectronic devices suitable for lower-cost production.

4. Experimental Section

Synthesis/Purification/Characterization of N-GQDs and NS-GQDs: A microwave-assisted method was used to synthesize N-GQDs and NS-GQDs by using a commercially available microwave. In a standard procedure, a 0.14 M aqueous solution of glucosamine-HCl was placed in a microwave for 40 min at 450 W. Additionally in the production of NS-GQDs, thiourea was used as a source of sulfur, with a ratio 1:1 of glucosamine-HCl to thiourea. As prepared graphene quantum dots were collected and purified utilizing bag dialysis with 500–1000 Da membrane for seven days as the DI water dialyzed against was replaced daily. After such purification, a synthesis yield of 15–20% was achieved. Following the purification, Benedict's test[78,79] was performed to verify whether the unreacted glucosamine precursor was still present in the product. This test was prequantified to detect glucosamine at concentrations of over 0.15 mg mL^{-1} (Figure S13a, Supporting Information). As a result, unpurified graphene quantum dots showed a positive indication of glucosamine presence whereas for the purified product the test was always negative indicating minimal to a negligible concentration of glucosamine precursor in the suspension of purified quantum dots (Figure S13b, Supporting Information).

N-GQDs and NS-GQDs were morphologically characterized by using TEM (TEM JEOL JEM-2100). Samples for TEM were prepared on the carbon-coated 200-mesh copper grid under ambient conditions. Optical characterization was done via absorption, fluorescence, and infrared spectroscopy (FTIR). Fluorescence spectra were measured using SPEX NanoLog, Horiba Scientific spectrofluorometer in the regions of 300 to 1000 nm with the excitation varied from 280 to 800 nm. Absorbance was recorded in the range of 200 to 800 nm with Agilent Technologies (Cary 60 UV-Vis) absorption spectrometer. In order to assess the functionalities of N-GQDs and NS-GQDs, the samples were freeze-dried in Labconco, FreeZone 4.5 freeze-dryer and analyzed in the ATR mode of the Thermo Nicolet Nexus 670 FTIR which allowed to reduce the water background. Raman spectrometer (DeltaNu) was used to characterize the GQDs with 785 nm excitation at 100 mW peak power. We spin-coated the solution-based GQDs on a silicon wafer at 1000 rpm for 30 s to prepare the sample for the Raman spectroscopic measurements. We utilized the tapping mode AFM (NT-MDT nanosolver) to measure the thickness of both GQDs. Aqueous GQDs were spin-coated three times at 3000 rpm for 30 s (each time) on a silicon chip substrate to prepare the samples for AFM measurements.

Calculation of QY: A comparative approach was followed to calculate the quantum yield of N-GQDs/NS-GQDs choosing Coumarin-153 in ethanol (47% QY at 400 nm excitation) and fluorescein in 0.1 M NaOH (92% QY at 360 nm excitation) as reference materials. We use the following formula to find the QY of both GQDs

$$\Phi_{GQDs} = \Phi_{ref} \times \left(\frac{FLI_{GQDs}}{FLI_{ref}}\right) \times \left(\frac{Abs_{ref}}{Abs_{GQDs}}\right) \times \left(\frac{\eta_{GQDs}}{\eta_{ref}}\right)^2 \quad (1)$$

In the above expression, Φ_{ref} denotes the quantum yield of respective materials, FLI represents the experimentally measured integrated fluorescence intensity, Abs indicates the absorbance of materials at the excitation wavelength, and η is denoted as the refractive index of the solvents. The refractive indexes of water, Coumarin-153, and Fluorescein are considered as 1.33, 1.36, and 1.33, respectively.

Device Fabrication: ITO-coated glass electrode was used as a substrate for the device fabrication. ITO glass was cleaned by using 10% HCl for 1 h and ultrasonic treatment cleaning in acetone for 1 h, after which it was blow dried using N_2 gas. Prior to deposition on the ITO glass PEDOT: PSS at a concentration 1.1 wt% in water with a ratio of 1:1 PEDOT to PSS was filtered using a 0.45 µm pore size syringe filter, and ultrasonically dispersed in an ultrasonic bath for 30 min. Further 200 µL of PEDOT: PSS solution was spun on ITO glass at 3000 rpm for 20 s, then the sample was baked in an oven at 120 °C for 1 h. N-GQDs and NS-GQDs were deposited on the ITO-PEDOT:PSS by spin-coating 300 µL of 5 mg mL^{-1} aqueous suspension of N-GQDs or NS-GQDs at 3000 rpm for 20 s, followed by annealing 120 °C for 1 h. Finally, silver paste was deposited on the top of the device to make the electrical contacts. Prior to electrical testing, the morphology of the devices was characterized via scanning electron microscopy (JEOL-JSM-7100F). For the electroluminescence experiments, the source and drain of the devices were connected to Harrison 6205B DC power supply and voltages up to 15 V was applied to provide electron and hole current. The device was placed inside the Horiba Spex Nanolog fluorescence spectrometer to assess the electroluminescence emission as the bias was applied. The photoluminescence of the devices was measured using the Ocean Optics (S2000) spectrometer at 365 nm excitation wavelength. The Keithley 2420 Source Meter Unit instrument was utilized to measure the turn-on voltage of both devices.

Supporting Information

Supporting Information is available from the Wiley Online Library or from the author.

Acknowledgements

MdT.H. and R.G.-R. contributed equally to this work. The authors would like to thank TCU for providing funding from the TCU Research and

Creative Activities Fund, and TCU Invests in Scholarship grant funding. This work was partially supported by a grant from the Robert A. Welch Foundation (Grant P-1212 to J.L.C.) as well.

Conflict of Interest

The authors declare no conflict of interest.

Keywords

electroluminescence, graphene quantum dots, NIR fluorescence, quantum yield, visible fluorescence

Received: June 24, 2018
Revised: August 6, 2018
Published online: August 30, 2018

[1] A. K. Geim, *Science* **2009**, *324*, 1530.
[2] Y. Okigawa, K. Tsugawa, T. Yamada, M. Ishihara, M. Hasegawa, *Appl. Phys. Lett.* **2013**, *103*, 153106.
[3] X. Ma, H. Zhang, *Nanoscale Res. Lett.* **2013**, *8*, 440.
[4] A. K. Geim, K. S. Novoselov, *Nat. Mater.* **2007**, *6*, 183.
[5] J. K. Wassei, R. B. Kaner, *Mater. Today* **2010**, *13*, 52.
[6] K. P. Loh, Q. Bao, G. Eda, M. Chhowalla, *Nat. Chem.* **2010**, *2*, 1015.
[7] H. Md Tanvir, J. S. Brian, M. Price, R. Conor, D. Hung, G. Zygmunt, V. N. Anton, *Nanotechnology* **2017**, *28*, 065705.
[8] L. Tang, R. Ji, X. Cao, J. Lin, H. Jiang, X. Li, K. S. Teng, C. M. Luk, S. Zeng, J. Hao, S. P. Lau, *ACS Nano* **2012**, *6*, 5102.
[9] J. Peng, W. Gao, B. Gupta, Z. Liu, R. Romero-Aburto, L. Ge, *Nano Lett.* **2012**, *2*, 844.
[10] J. Lu, J.-X. Yang, J. Wang, A. Lim, S. Wang, K. P. Loh, *ACS Nano* **2009**, *3*, 2367.
[11] B. V. Senkovskiy, M. Pfeiffer, S. K. Alavi, A. Bliesener, J. Zhu, S. Michel, A. V. Fedorov, R. German, D. Hertel, D. Haberer, L. Petaccia, F. R. Fischer, K. Meerholz, P. H. M. van Loosdrecht, K. Lindfors, A. Grüneis, *Nano Lett.* **2017**, *17*, 4029.
[12] J.-L. Chen, X.-P. Yan, K. Meng, S.-F. Wang, *Anal. Chem.* **2011**, *83*, 8787.
[13] A. Naumov, F. Grote, M. Overgaard, A. Roth, C. E. Halbig, K. Nørgaard, D. M. Guldi, S. Eigler, *J. Am. Chem. Soc.* **2016**, *138*, 11445.
[14] R. Ye, Z. Peng, A. Metzger, J. Lin, J. A. Mann, K. Huang, C. Xiang, X. Fan, E. L. G. Samuel, L. B. Alemany, A. A. Martí, J. M. Tour, *ACS Appl. Mater. Interfaces* **2015**, *7*, 7041.
[15] L. Wang, Y. Wang, T. Xu, H. Liao, C. Yao, Y. Liu, Z. Li, Z. Chen, D. Pan, L. Sun, M. Wu, *Nat. Commun.* **2014**, *5*, 5357.
[16] R. Ye, C. Xiang, J. Lin, Z. Peng, K. Huang, Z. Yan, N. P. Cook, E. L. G. Samuel, C.-C. Hwang, G. Ruan, G. Ceriotti, A.-R. O. Raji, A. A. Martí, J. M. Tour, *Nat. Commun.* **2013**, *4*, 2943.
[17] S. Zhu, Y. Song, J. Wang, H. Wan, Y. Zhang, Y. Ning, B. Yang, *Nano Today* **2017**, *13*, 10.
[18] J. Sun, S. Yang, Z. Wang, H. Shen, T. Xu, L. Sun, H. Li, W. Chen, X. Jiang, G. Ding, Z. Kang, X. Xie, M. Jiang, *Part. Part. Syst. Charact.* **2015**, *32*, 434.
[19] F. Niu, Y. Xu, J. Liu, Z. Song, M. Liu, J. Liu, *Electrochim. Acta* **2017**, *236*, 239.
[20] Q. Liu, B. Guo, Z. Rao, B. Zhang, J. R. Gong, *Nano Lett.* **2013**, *13*, 2436.
[21] M. Nurunnabi, Z. Khatun, K. M. Huh, S. Y. Park, D. Y. Lee, K. J. Cho, Y.-k. Lee, *ACS Nano* **2013**, *7*, 6858.
[22] L. Zhou, J. Geng, B. Liu, *Part. Part. Syst. Charact.* **2013**, *30*, 1086.
[23] X. Zhu, T. Zhao, Z. Nie, Z. Miao, Y. Liu, S. Yao, *Nanoscale* **2016**, *8*, 2205.
[24] J. Qiu, R. Zhang, J. Li, Y. Sang, W. Tang, P. Rivera Gil, H. Liu, *Int. J. Nanomed.* **2015**, *10*, 6709.
[25] S. Coe, W.-K. Woo, M. Bawendi, V. Bulovi , *Nature* **2002**, *420*, 800.
[26] N. Tessler, V. Medvedev, M. Kazes, S. Kan, U. Banin, *Science* **2002**, *295*, 1506.
[27] D. I. Son, B. W. Kwon, D. H. Park, W.-S. Seo, Y. Yi, B. Angadi, C.-L. Lee, W. K. Choi, *Nat. Nanotechnol.* **2012**, *7*, 465.
[28] A. J. Nozik, *Nanostructures* **2002**, *14*, 115.
[29] I. Gur, N. A. Fromer, M. L. Geier, A. P. Alivisatos, *Science* **2005**, *310*, 462.
[30] Y. Li, Y. Hu, Y. Zhao, G. Shi, L. Deng, Y. Hou, *Adv Mater* **2011**, *23*, 776.
[31] A. P. Alivisatos, W. Gu, C. Larabell, *Annu. Rev. Biomed. Eng.* **2005**, *7*, 55.
[32] S. Zhu, J. Zhang, C. Qiao, S. Tang, Y. Li, W. Yuan, B. Li, L. Tian, F. Liu, R. Hu, H. Gao, H. Wei, H. Zhang, H. Sun, B. Yang, *Chem. Commun.* **2011**, *47*, 6858.
[33] Z. Fan, S. Li, F. Yuan, L. Fan, *RSC Adv.* **2015**, *5*, 19773.
[34] R. Xie, Z. Wang, W. Zhou, Y. Liu, L. Fan, Y. Li, X. Li, *Anal. Methods* **2016**, *8*, 4001.
[35] M. K. Kumawat, M. Thakur, R. B. Gurung, R. Srivastava, *Sci. Rep.* **2017**, *7*, 15858.
[36] Z. L. Wu, M. X. Gao, T. T. Wang, X. Y. Wan, L. L. Zheng, C. Z. Huang, *Nanoscale* **2014**, *6*, 3868.
[37] Z. Zeng, S. Chen, T. T. Y. Tan, F.-X. Xiao, *Catal. Today* **2018**, *315*, 171.
[38] D. Pan, C. Xi, Z. Li, L. Wang, Z. Chen, B. Lu, M. Wu, *J. Mater. Chem. A* **2013**, *1*, 3551.
[39] X. Deng, J. Sun, S. Yang, H. Shen, W. Zhou, J. Lu, G. Ding, Z. Wang, *Appl. Phys. Lett.* **2015**, *107*, 241905.
[40] C.-T. Hsieh, D.-Y. Tzou, K.-Y. Hsieh, K.-M. Yin, *RSC Adv.* **2017**, *7*, 18340.
[41] Y. Li, Y. Zhao, H. Cheng, Y. Hu, G. Shi, L. Dai, L. Qu, *J. Am. Chem. Soc.* **2012**, *134*, 15.
[42] R. Gokhale, P. Singh, *Part. Part. Syst. Charact.* **2014**, *31*, 433.
[43] Q. Li, S. Zhang, L. Dai, L.-s. Li, *J. Am. Chem. Soc.* **2012**, *134*, 18932.
[44] L.-J. Wang, H.-O. Li, T. Tu, G. Cao, C. Zhou, X.-J. Hao, Z. Su, M. Xiao, G.-C. Guo, A. M. Chang, G.-P. Guo, *Appl. Phys. Lett.* **2012**, *100*, 022106.
[45] W. Kwon, Y.-H. Kim, C.-L. Lee, M. Lee, H. C. Choi, T.-W. Lee, S.-W. Rhee, *Nano Lett.* **2014**, *14*, 1306.
[46] J. Shen, Y. Zhu, C. Chen, X. Yang, C. Li, *Chem. Commun.* **2011**, *47*, 2580.
[47] J. Shen, Y. Zhu, X. Yang, J. Zong, J. Zhang, C. Li, *New J. Chem.* **2012**, *36*, 97.
[48] D. Pan, J. Zhang, Z. Li, M. Wu, *Adv Mater* **2010**, *22*.
[49] Z.-C. Yang, X. Li, J. Wang, *Carbon* **2011**, *49*, 5207.
[50] C.-Y. Teng, T.-F. Yeh, K.-I. Lin, S.-J. Chen, M. Yoshimura, H. Teng, *J. Mater. Chem. C* **2015**, *3*, 4553.
[51] T.-F. Yeh, W.-L. Huang, C.-J. Chung, I. T. Chiang, L.-C. Chen, H.-Y. Chang, W.-C. Su, C. Cheng, S.-J. Chen, H. Teng, *J. Phys. Chem. Lett.* **2016**, *7*, 2087.
[52] S. Kellici, J. Acord, N. P. Power, D. J. Morgan, P. Coppo, T. Heil, B. Saha, *RSC Adv.* **2017**, *7*, 14716.
[53] M. Zhang, L. Bai, W. Shang, W. Xie, H. Ma, Y. Fu, D. Fang, H. Sun, L. Fan, M. Han, C. Liu, S. Yang, *J. Mater. Chem.* **2012**, *22*, 7461.
[54] J. Ren, X. Dong, G. Zhang, T. Li, Y. Wang, *New J. Chem.* **2017**, *41*, 13961.
[55] G. Li, F. W. R. Rivarola, N. J. L. K. Davis, S. Bai, T. C. Jellicoe, F. d. l. Peña, S. Hou, C. Ducati, F. Gao, R. H. Friend, N. C. Greenham, Z. K. Tan, *Adv. Mater.* **2016**, *28*, 3528.
[56] B. Zheng, Y. Chen, P. Li, Z. Wang, B. Cao, F. Qi, J. Liu, Z. Qiu, W. Zhang, *Nanophotonics* **2017**, *6*, 259.

[57] D. Qu, M. Zheng, L. Zhang, H. Zhao, Z. Xie, X. Jing, R. E. Haddad, H. Fan, Z. Sun, *Sci. Rep.* **2014**, *4*, 5294.
[58] L. Hu, Y. Sun, S. Li, X. Wang, K. Hu, L. Wang, X.-j. Liang, Y. Wu, *Carbon* **2014**, *67*, 508.
[59] L. Zhimin, Q. Guangqin, C. Keyu, Z. Min, Y. Lihui, Z. Xinwen, H. Wei, W. Lianhui, *Adv. Funct. Mater.* **2016**, *26*, 2739.
[60] X. Hou, Y. Li, C. Zhao, *Aust. J. Chem.* **2016**, *69*, 357.
[61] S. Kumar, S. K. T. Aziz, O. Girshevitz, G. D. Nessim, *J. Phys. Chem. C* **2018**, *122*, 2343.
[62] G. Eda, Y.-Y. Lin, C. Mattevi, H. Yamaguchi, H.-A. Chen, I. S. Chen, C.-W. Chen, M. Chhowalla, **2010**, *22*, 505.
[63] L. Wang, S.-J. Zhu, H.-Y. Wang, S.-N. Qu, Y.-L. Zhang, J.-H. Zhang, Q.-D. Chen, H.-L. Xu, W. Han, B. Yang, H.-B. Sun, *ACS Nano* **2014**, *8*, 2541.
[64] L. Wang, H. Wang, Y. Wang, S. Zhu, Y. Zhang, J. Zhang, *Adv. Mater.* **2013**, *25*, 6539.
[65] Q. Xu, Q. Zhou, Z. Hua, Q. Xue, C. Zhang, X. Wang, D. Pan, M. Xiao, *ACS Nano* **2013**, *7*, 10654.
[66] J.-H. Sung, J. S. Yang, B.-S. Kim, C.-H. Choi, M.-W. Lee, S.-G. Lee, S.-G. Park, E.-H. Lee, B.-H. O, *Appl. Phys. Lett.* **2010**, *96*, 261105.
[67] D. Tordera, M. Delgado, E. Ortí, H. J. Bolink, J. Frey, M. K. Nazeeruddin, E. Baranoff, *Chem. Mater.* **2012**, *24*, 1896.
[68] Q. Yang, J. Duan, W. Yang, X. Li, J. Mo, P. Yang, Q. Tang, *Appl. Surf. Sci.* **2018**, *434*, 1079.
[69] H. Ding, J.-S. Wei, H.-M. Xiong, *Nanoscale* **2014**, *6*, 13817.
[70] S. Do, W. Kwon, Y.-H. Kim, S. R. Kang, T. Lee, T.-W. Lee, S.-W. Rhee, *Adv. Opt. Mater.* **2016**, *4*, 276.
[71] D. Qu, M. Zheng, P. Du, Y. Zhou, L. Zhang, D. Li, H. Tan, Z. Zhao, Z. Xie, Z. Sun, *Nanoscale* **2013**, *5*, 12272.
[72] L. Tang, R. Ji, X. Li, G. Bai, C. P. Liu, J. Hao, J. Lin, H. Jiang, K. S. Teng, Z. Yang, S. P. Lau, *ACS Nano* **2014**, *8*, 6312.
[73] M. T. Hasan, B. J. Senger, C. Ryan, M. Culp, R. Gonzalez-Rodriguez, J. L. Coffer, A. V. Naumov, *Sci. Rep.* **2017**, *7*, 6411.
[74] L. Bao, Z.-L. Zhang, Z.-Q. Tian, L. Zhang, C. Liu, Y. Lin, B. Qi, D.-W. Pang, *Adv. Mater.* **2011**, *23*, 5801.
[75] J. Shang, L. Ma, J. Li, W. Ai, T. Yu, G. G. Gurzadyan, *Sci. Rep.* **2012**, *2*, 792.
[76] X. Li, S. Zhang, S. A. Kulinich, Y. Liu, H. Zeng, *Sci. Rep.* **2014**, *4*, 4976.
[77] X. Wu, F. Tian, W. Wang, J. Chen, M. Wu, J. X. Zhao, *J. Mater. Chem. C* **2013**, *1*, 4676.
[78] S. R. Benedict, *J. Biol. Chem* **1931**, *92*.
[79] J. Park, O. C. Jeon, J. Yun, H. Nam, J. Hwang, T. A. Al-Hilal, K. Kim, K. Kim, Y. Byun, *J. Med. Chem.* **2016**, *59*, 10520.